JGP Journal of General Physiology

RESEARCH ARTICLE

An interaction between the III-IV linker and CTD in $Na_V1.5$ confers regulation of inactivation by CaM and FHF

Aravind R. Gade[1], Steven O. Marx[2,3], and Geoffrey S. Pitt[1]

Voltage gated sodium channel (VGSC) activation drives the action potential upstroke in cardiac myocytes, skeletal muscles, and neurons. After opening, VGSCs rapidly enter a non-conducting, inactivated state. Impaired inactivation causes persistent inward current and underlies cardiac arrhythmias. VGSC auxiliary proteins calmodulin (CaM) and fibroblast growth factor homologous factors (FHFs) bind to the channel's C-terminal domain (CTD) and limit pathogenic persistent currents. The structural details and mechanisms mediating these effects are not clear. Building on recently published cryo-EM structures, we show that CaM and FHF limit persistent currents in the cardiac $Na_V1.5$ VGSC by stabilizing an interaction between the channel's CTD and III-IV linker region. Perturbation of this intramolecular interaction increases persistent current and shifts the voltage dependence of steady-state inactivation. Interestingly, the $Na_V1.5$ residues involved in the interaction are sites mutated in the arrhythmogenic long QT3 syndrome (LQT3). Along with electrophysiological investigations of this interaction, we present structural models that suggest how CaM and FHF stabilize the interaction and thereby limit the persistent current. The critical residues at the interaction site are conserved among VGSC isoforms, and subtle substitutions provide an explanation for differences in inactivation among the isoforms.

Introduction

Voltage-gated sodium channels (VGSCs) are primarily expressed in excitable cells such as neurons, skeletal muscles, and cardiac myocytes, where they initiate action potentials. VGSCs are large proteins consisting of four transmembrane domains (DI–DIV), each containing six transmembrane-spanning α-helices (S1–S6), connected through intracellular linkers and capped with an intracellular N-terminal domain and an intracellular C-terminal domain (CTD; Catterall, 2000). Each transmembrane domain consists of a voltage sensor (S1–S4) while S5 and S6 line the channel pore (Fig. 1 A). Mammals express nine subtypes ($Na_V1.1$–1.9) of VGSCs, each with a different tissue distribution (Catterall et al., 2005). $Na_V1.5$ is the primary subtype of VGSC in cardiac myocytes (Gellens et al., 1992).

VGSCs are fast-activating and -inactivating. After channel activation opens the channel pore, the hydrophboic IFM motif (amino acids isoleucine, phenylalanine, and methionine) within the III-IV linker bind to a hydrophobic pocket between domains III and IV to drive fast inactivation by allosterically blocking the pore (Shen et al., 2018; West et al., 1992; Yan et al., 2017b). Mutations in the IFM motif or in the surrounding residues on the III-IV linker can impair inactivation leading to a persistent inward current (Bennett et al., 1995; Patton et al., 1992) that has pathological consequences. For example, increased persistent current in $Na_V1.2$ or $Na_V1.6$ leads to epilepsy; in $Na_V1.5$ it causes congenital Long QT syndrome type 3 (LQT3) as well as acquired long QT syndrome (Choi et al., 2016; Kapplinger et al., 2015; Meisler and Kearney, 2005; Wang et al., 1995; Wu et al., 2011).

Pathological mutations in other intracellular VGSC domains can also increase the persistent current, presumably by directly or allosterically affecting the III-IV linker's function, yet the specific mechanisms remain unknown. In $Na_V1.5$, the CTD is a particular hotspot for pathological arrhythmia-associated mutations that impair inactivation (Kapplinger et al., 2015; Musa et al., 2015; Yan et al., 2017a). The CTD serves as the binding site for VGSC auxiliary proteins such as calmodulin (CaM) and fibroblast growth factor homologous factors (FHFs; Pitt and Lee, 2016), both of which have been implicated in the regulation of persistent current. Arrhythmia-associated mutations hindering the binding of CaM increase the VGSC persistent current, which can be reduced by overexpression of CaM to overcome the

[1]Cardiovascular Research Institute, Weill Cornell Medicine, New York, NY; [2]Division of Cardiology, Department of Medicine, Vagelos College of Physicians and Surgeons, Columbia University, New York, NY; [3]Department of Pharmacology, Vagelos College of Physicians and Surgeons, Columbia University, New York, NY.

Correspondence to Geoffrey S. Pitt: geoffrey.pitt@med.cornell.edu.

https://doi.org/10.1085/jgp.201912434

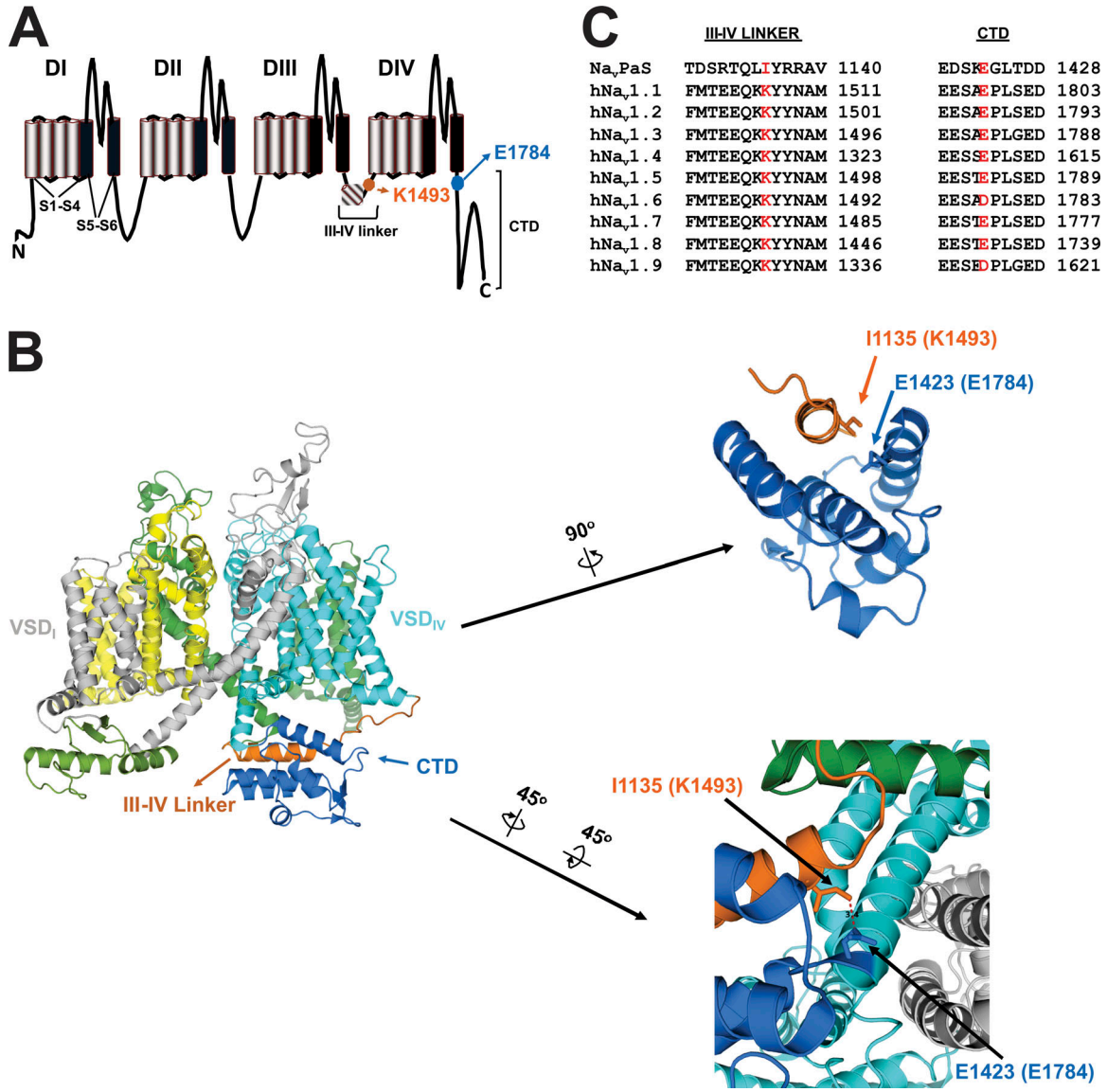

Figure 1. **Putative interaction site between CTD and III-IV linker. (A)** Schematic of a VGSC displaying the location of the amino acids involved in the putative interaction site (numbering per Na$_V$1.5). VSD refers to voltage sensor domain. **(B)** Structure of Na$_V$Pas (PDB accession no. 5X0M) as seen from the membrane. The putative interaction site is displayed in the zoomed-in images. **(C)** Sequence homology among different subtypes of human VGSCs and Na$_V$Pas surrounding the amino acids involved in the putative interaction, which are marked in red.

reduced binding affinity for those mutants (Yan et al., 2017a). Similarly, mutations that affect the binding of FHFs to the CTD increase the persistent current, leading to arrhythmias (Musa et al., 2015).

While those examples provide insight into the mechanisms by which CTD mutations increase persistent current, they do not indicate how the CTD through its auxiliary proteins ultimately modulates the III-IV linker to affect inactivation. One hypothesis is that CTD directly interacts with the III-IV linker (Motoike et al., 2004). Such an interaction was recently confirmed in a full-length VGSC by the Na$_V$Pas cryo-EM structure. Captured in a closed conformation with the voltage sensors up, the model showed that an α-helix in the III-IV linker falls into groove among α-helices in the CTD, like a hot dog in a bun (Fig. 1 B). In this arrangement, the δ carbon of I1135 in the III-IV linker is 3.4 Å from the γ carbon of E1423 in the CTD (Shen et al., 2017; Fig. 1 B). This interaction between the III-IV linker and the CTD appears to be dynamic because the III-IV linker adopts a markedly different conformation in other VGSC structures captured in inactivated conformations (Pan et al., 2019; Shen et al., 2018, 2019; Yan et al., 2017b). The discovery of this dynamic interaction between the III-IV linker and the CTD residue E1423, which corresponds to E1784 in Na$_V$1.5 (Fig. 1 D), is intriguing because E1784K is the most commonly reported mutation in LQT3 (Kapplinger et al., 2015), for which increased persistent current is major biophysical defect (Makita et al., 2008; Wei et al., 1999). Indeed, previous reports show that E1784K confers a large persistent sodium current (Makita et al., 2008; Peters et al., 2017; Wei et al., 1999).

We therefore used the Na$_V$Pas structure as a starting point to explore whether an analogous interaction between the III-IV

Table 1. **Summary of steady-state inactivation properties**

$Na_V1.5$ (Control or CaM overexpressed)	$V_{1/2}$ inactivation	*k*	*n*
WT	−83.2 ± 1.2	4.9 ± 0.1	26
+ CaM	−84.7 ± 1.8	4.8 ± 0.1	14
K1493A	−80.4 ± 1.5	4.6 ± 0.1	9
+ CaM	−82.1 ± 6.6	4.4 ± 0.3	5
K1493E	−88.7 ± 0.7[a]	5.0 ± 0.1	31
+ CaM	−88.5 ± 0.8[a]	5.1 ± 0.1	8
E1784K	−91.5 ± 0.9[a]	6.6 ± 0.2	18
+ CaM	−88.6 ± 1.1[a]	6.1 ± 0.1	6
K1493A+E1784K	−84.7 ± 2.3[b]	6.0 ± 0.2	10
+ CaM	−85.8 ± 2.0[b]	6.3 ± 0.2	5
K1493E+E1784K	−87.6 ± 0.8[a,b]	6.2 ± 0.1	27
+ CaM	−87.4 ± 0.8[a,b]	5.9 ± 0.1	14
K1505N	−87.6 ± 1.4[a]	4.8 ± 0.2	9
+ CaM	−89.3 ± 2.3[a]	5.0 ± 0.1	8
K1505E	−90.8 ± 1.5[a]	5.1 ± 0.2	9
+ CaM	−87.5 ± 1.3[a]	5.3 ± 0.2	8
K1493I	−82.4 ± 1.8[b]	4.7 ± 0.1	7
K1493I+E1784K	−82.9 ± 2.6[b]	5.3 ± 0.1	7
K1492E	−81.7 ± 1.4	4.3 ± 0.1	10
K1492E+E1784K	−87.5 ± 1.8	5.7 ± 0.2	19

Data presented as mean ± SEM.
[a]$P < 0.05$ compared to WT.
[b]$P < 0.05$ compared to E1784K.

linker and the CTD is present in $Na_V1.5$, and whether that interaction contributes to the mechanisms by which the CTD affects channel inactivation. The amino acid in $Na_V1.5$ corresponding to I1135 in the III-IV linker of Na_VPas is K1493 (Fig. 1 C). The potential significance of the III-IV linker to CTD interaction is underscored by conservation of both K1493 and E1784 among the different subtypes of mammalian VGSCs (Fig. 1 C) and because both are sites in $Na_V1.5$ for LQT3 mutations (Kapplinger et al., 2015; Zumhagen et al., 2013), suggesting that disruption of the interaction adversely affects channel function. Because mutations at K1493 have been linked to LQT3, electrophysiological recordings of K1493 substitutions would be predicted to increase persistent current, but such data have not been reported. A K1493 deletion mutant, discovered in a large family with sudden cardiac death, was studied in HEK293 cells and found to produce decreased voltage-dependent Na^+ currents (Zumhagen et al., 2013). It was separately discovered in the parent of a proband with compound mutations, and in that study, mutant channels did not support Na^+ current (Nof et al., 2019). The critical role of E1784 and its interaction with the III-IV linker is further highlighted because E1784K is also the most commonly reported Brugada syndrome mutation (Kapplinger et al., 2015). Here, we tested whether the interaction between the III-IV linker and CTD occurs in $Na_V1.5$ and whether it affects persistent current. With this background, we then tested whether this interaction helps explain the contribution of the CTD-interacting auxiliary subunits CaM and FHF to regulating persistent current.

Materials and methods

HEK cell culture and transfection

HEK293 cells maintained in Dulbecco's modified Eagle's medium with 1 g/liter glucose at 37°C were used for transfection. Lipofectamine 2000 (Invitrogen) protocol was followed for transfection. For experiments with $Na_V1.5$ Δ1885 mutations, the total amount of cDNA used was 3 µg of WT or Δ1885 $Na_V1.5$, 2 µg of CaM or FGF12B or FGF13B or FGF13B (R57A) or empty vector, along with 0.5 µg of eGFP. For experiments with mutations at the interaction site (on III-IV linker and CTD) the total amount of cDNA used was 3 µg of WT or mutant $Na_V1.5$, 1.5 µg of β1 subunit, 2 µg of CaM or FGF12B or empty vector along with 0.5 µg of enhanced GFP (eGFP). Since a previous report suggested that the Na_V β1 subunit can affect Ca^{2+}/CaM-dependent regulation of $Na_V1.5$ (Nof et al., 2019), we tested specifically whether coexpression of Na_V β1 affected $Na_V1.5$ persistent current under Ca^{2+} chelated conditions—one of our main readouts in this study. Fig. S1 shows that expression of β1 had no effect on persistent current for either of two $Na_V1.5$ disease mutants that display increased persistent current. For experiments with mutations on

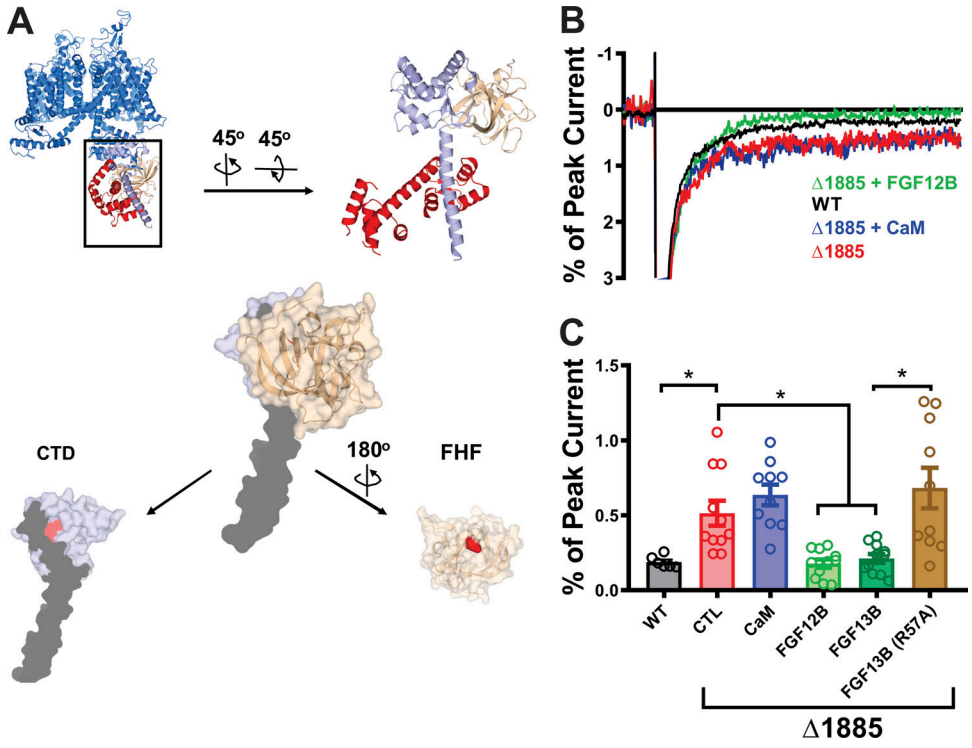

Figure 2. **FGF12B and FGF13B, but not CaM, are effective in rescuing persistent current in the Δ1885 mutant $Na_V1.5$ channels. (A)** Structure of the $Na_V1.5$ CTD overlaid on Na_VPas, with a zoomed-in view of the CTD (sky blue) along with CaM (red) and FGF13 (beige). The truncated protein in the Δ1885 mutant is shown in black. Below is the structure of the $Na_V1.5$ CTD (blue), displaying the truncated portion in black, and the critical site for FHF binding in red (H1849), and the structure of FHF displaying the amino acid (R57) critical for the interaction with VGSC CTDs, shown in red. **(B)** Exemplar traces displaying the persistent currents in WT and mutant $Na_V1.5$ channels. **(C)** Quantified data from WT and mutant $Na_V1.5$ channels. *, $P < 0.05$. CTL refers to "control," i.e., no additional protein expressed.

$Na_V1.6$, the total amount of cDNA used was 5 µg of WT or mutant $Na_V1.6$, 1.5 µg of β1 subunit, and 1.5 µg of β2 subunit, along with 0.5 µg of eGFP. Cells were transfected in media containing Lipofectamine 2000 for 4 h ($Na_V1.5$) or overnight ($Na_V1.6$) before changing the media. Cells were replated on coverslips for electrophysiological recordings 24 h after transfection. Coexpression of the auxiliary subunits has been previously validated in HEK cells by our laboratory (Musa et al., 2015; Pablo et al., 2016; Wang et al., 2011, 2012; Yan et al., 2017a).

Electrophysiological recordings

All recordings were made at room temperature (~23°C). A HEKA EPC 10 amplifier (USB) was used to acquire whole-cell voltage clamp recordings. Recordings were made from cells perfused with external solution containing (in mM) 124 NaCl, 5 KCl, 2 $CaCl_2$, 1 $MgCl_2$, 20 TEA-Cl, 5 HEPES, and 10 glucose. NaOH was added to achieve pH 7.4. Borosilicate glass pipettes were filled with (in mM) 125 CsF, 10 NaCl, 10 HEPES, 15 TEA-Cl, 1.1 EGTA, and 0.5 Na-GTP, adjusted to pH 7.3, and patched onto the cells. Pipettes were prepared using a P-97 pipette puller (Sutter Instruments). Resistance of pipettes was 1–1.5 MΩ. Chemicals used for external and internal solutions were purchased from Sigma-Aldrich except tetrodotoxin (TTX; Cayman Chemicals). To obtain I-V curves, cells were depolarized to a series of voltages ranging from −90 mV to +55 mV from a holding potential of −120 mV. To obtain the peak current and persistent current values, cells were held at a voltage of −120 mV and depolarized to −20 mV. Peak currents of the cells were less than −7.5 nA. Persistent current values were obtained by averaging the current 150–155 ms after stimulation and are presented as percentage of peak current. The time constants for fast inactivation were calculated with a single exponential fit 5–95% of the peak current obtained at −20 mV. To obtain the activation curves, current data were converted to G with equation $G = I_{Na} / (E_m - E_{Rev})$, where I_{Na} is the peak sodium current, E_m is membrane potential, and E_{Rev} is the reversal potential for Na^+. Conductance values were then fitted with a Boltzman equation $[G / G_{max} = (1 + \exp((V_{1/2} - V) / k))^{-1}]$, where G_{max} is the maximum conductance, $V_{1/2}$ is the half-activation voltage, V is the test voltage, and k is the slope. To obtain the steady-state inactivation curves, currents were elicited at −20 mV for 20 ms following a 500-ms prepulse to voltages ranging from −120 to +20 mV from a holding voltage of −120 mV. Normalized values obtained at −20 mV pulse were used to plot the steady-state inactivation curves. A Boltzmann equation $[I/I_{max} = (1 + \exp((V - V_{1/2}) / k))^{-1}]$, where I_{max} is the maximum current, $V_{1/2}$ is half-inactivation voltage, and k is the slope was used to fit the data and calculate the $V_{1/2}$ of inactivation. Activation and inactivation data are summarized in Table 1, Table S1, and Fig. S2.

Statistical analysis

Data analysis was performed using GraphPad Prism 8.0 and Microsoft Excel software. All averaged data are presented as

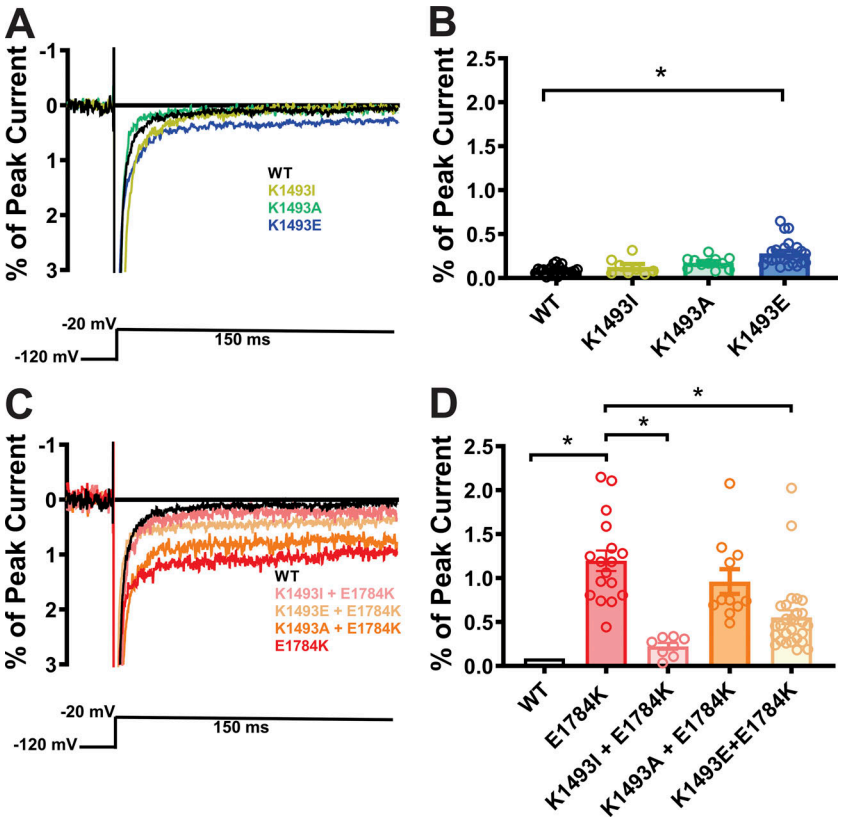

Figure 3. **Mutations at the putative interaction site lead to an increased persistent current. (A and C)** Exemplar traces displaying the persistent currents in WT and mutant VGSCs. **(B and D)** Quantified data of persistent currents from WT and mutant VGSCs. Gray column with black outline in D represents the WT data from B (common for both, with graphs on a different scale). *, P < 0.05.

mean ± SEM. Statistical significance was determined using one-way ANOVA, Newman–Keuls multiple comparison test, and unpaired *t* test. P values of ≤0.05 were considered statistically significant.

Online supplemental material

Fig. S1 shows the effects of β1 subunit on the persistent currents in K1493E and E1784K mutants. Fig. S2 shows conductance-voltage curves for WT and mutant VGSCs. Figs. S3 and S4 show exemplary traces and IV curves for WT and mutant VGSCs. Fig. S5 shows the involvement of other potential sites of interaction between CTD and III-IV linker in CaM and FHF modulation of Nav1.5 channel. Fig. S6 shows the inactivation time constant data from WT and mutant VGSCs.

Results

Effects of apocalmodulin (apoCaM) and FHFs on $Na_V1.5$ persistent currents are mediated through the $Na_V1.5$ CTD

We started our analysis by defining requirements for CaM modulation of $Na_V1.5$ persistent Na^+ current. A previous study showed that persistent Na^+ current associated with LQT3 mutations in the CTD could be reduced when CaM was overexpressed, consistent with the mutations' effects on reducing affinity between the CTD and CaM. Those studies were performed with high concentrations of EGTA in the intracellular patch pipette, and thus queried the role of apoCaM (Yan et al., 2017a). During nondiseased states, $Na_V1.5$ channels open rapidly and inactivate quickly at the beginning of the cardiac action potential, which is before cytosolic Ca^{2+} rises from either influx through voltage-gated Ca^{2+} channels or release from the sarcoplasmic reticulum. Thus, absent aberrant increases in basal cytosolic Ca^{2+}, a role for Ca^{2+}-dependent regulation of persistent Na^+ current through CaM is unlikely. Crystal structures of CaM and an FHF bound to the CTD and obtained in the absence of Ca^{2+} show that the CaM C-lobe binds to a long α-helix starting at T1896 that contains the apoCaM binding "IQ" motif (Wang et al., 2012, 2014). Nevertheless, because studies suggest that CaM can also interact directly with the III-IV linker, albeit in a Ca^{2+}-dependent manner (Johnson et al., 2018; Sarhan et al., 2012), we tested whether the reduction in persistent current by CaM for LQT3 mutations in the CTD depended specifically upon CaM's interaction with the CTD. We exploited a previous study (Cormier et al., 2002) that showed that truncation of $Na_V1.5$ at amino acid 1885 (Δ1885), which eliminates the CaM-binding IQ motif (Fig. 2 A) and CaM interaction with the CTD (Wang et al., 2011), generates a large persistent current and a decrease in peak currents (Fig. S3), as previously shown (Biswas et al., 2009; Cormier et al., 2002). Thus, we expressed WT $Na_V1.5$ or Δ1885 along with $Na_V\beta1$ subunit and eGFP (to identify transfected cells) in HEK293 cells and tested whether, analogous to other mutations in the CTD that increase persistent current, overexpression of CaM could reduce the persistent current for Δ1885 (Fig. 2 C). Our experiments were performed with high concentrations of EGTA (10 mM) in the intracellular pipette solution, thus assuring that we were querying the effects of intracellular apoCaM, as was done previously (Yan et al., 2017a). Consistent with the previous analysis of Δ1885, we observed a persistent current that was significantly larger than for the WT $Na_V1.5$ (Fig. 2, C and D). CaM overexpression was unable to reduce the persistent current for Δ1885, however (Fig. 2 D). Although previous reports suggest

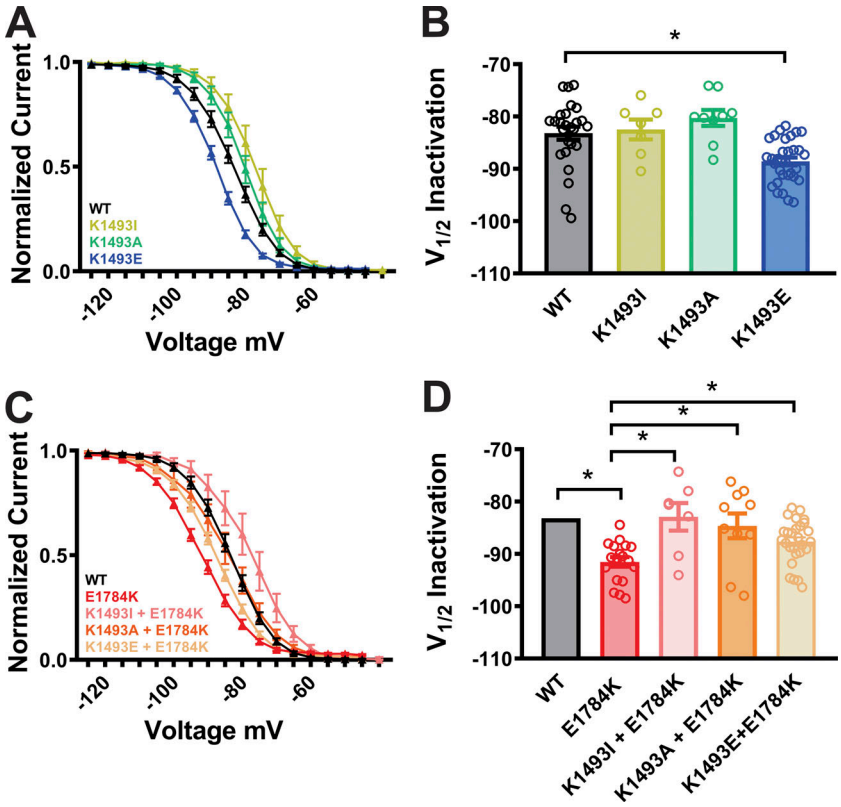

Figure 4. **Mutations at the putative interaction site lead to hyperpolarized shift in steady-state inactivation. (A and C)** Steady-state inactivation curves from WT and mutant channels. **(B and D)** Quantified data of $V_{1/2}$ of inactivation from WT and mutant channels. Gray column with black outline in D represents the WT data from B (common for both). *, $P < 0.05$.

that CaM interaction with the III-IV linker requires Ca^{2+} (Johnson et al., 2018; Sarhan et al., 2012), our results with Δ1885 suggest that in the context of low intracellular Ca^{2+}, the ability of apoCaM to reduce persistent current is dependent specifically on apoCaM's interactions with the CTD.

We then tested whether FHFs likewise required interaction with the CTD to reduce persistent current in $Na_V1.5$. As illustrated in Fig. 2 B, the Δ1885 truncation eliminates a portion of the FHF interaction surface on the CTD, yet retains a critical binding pocket for an arginine (R57 in FGF13B) that protrudes from the FHF surface and makes a major contribution to the interaction with the CTD (Musa et al., 2015; Pablo et al., 2016). Addition of either FGF12B or FGF13B reduced the persistent Na^+ current to the level observed for the intact channel, yet an R57A mutant of FGF13B, previously shown to specifically disrupt binding to the $Na_V1.5$ CTD (Musa et al., 2015; Pablo et al., 2016), was unable to reduce persistent current in Δ1885. Thus, the ability of either CaM or an FHF to modulate persistent current depended upon interaction between the auxiliary subunit and the CTD.

Mutations at the putative III-IV linker to CTD interaction site increase the persistent currents of the $Na_V1.5$ channel

Having shown that the CaM and FHF auxiliary subunits modulate persistent current through their interactions on the CTD, we sought a mechanism by which these CTD interactions affected the III-IV linker and persistent current. We focused on the putative interaction between the III-IV linker and the CTD observed in the closed-state Na_VPas structure (Shen et al., 2017), and hypothesized that the interaction stabilizes the closed state and thereby reduces persistent current. To test whether this interaction occurs in $Na_V1.5$, we recorded currents from WT and mutant $Na_V1.5$ channels designed to break or restore the interaction. We first examined mutations on the III-IV linker at K1493. We replaced K1493 with Ile, the corresponding nonconserved amino acid in Na_VPas. $Na_V1.5$ with K1493I did not show a significant difference in the persistent current compared with WT $Na_V1.5$ (Fig. 3, A and B). Although attempted recordings from Na_VPas did not yield functional Na^+ currents (Shen et al., 2017), these data suggest that the interaction observed between I1135 in the III-IV linker and E1432 in the CTD of Na_VPas supports a channel with limited persistent current. When we replaced K1493 with Glu (K1493E), which swaps the positively charged Lys side chain for the negatively charged long Glu side chain, we observed a significant increase in the persistent current (Fig. 3, A and B). In contrast, mutating the K1493 in $Na_V1.5$ to Ala (K1493A) did not increase the persistent current, suggesting that eliminating most of the Lys side chain and its positive charge at K1493 did not destabilize the III-IV linker and its allosteric closing of the channel pore and thus did not affect the interaction with E1784 in the CTD.

In the K1493E mutant, we suspected that the negatively charged Glu side chain at amino acid 1493 repelled and destabilized the interaction with negatively changed Glu at E1784. To test that hypothesis, we attempted to restore the interaction at amino acid 1784 by eliminating the presence of two positively charged side chains. We started by examining E1784K as the sole mutation in $Na_V1.5$. As reported previously (Makita et al., 2008; Wei et al., 1999), E1784K conferred a significant decrease in current density (Fig. S4), thus providing some context to why E1784K is also a leading Brugada syndrome–associated mutation

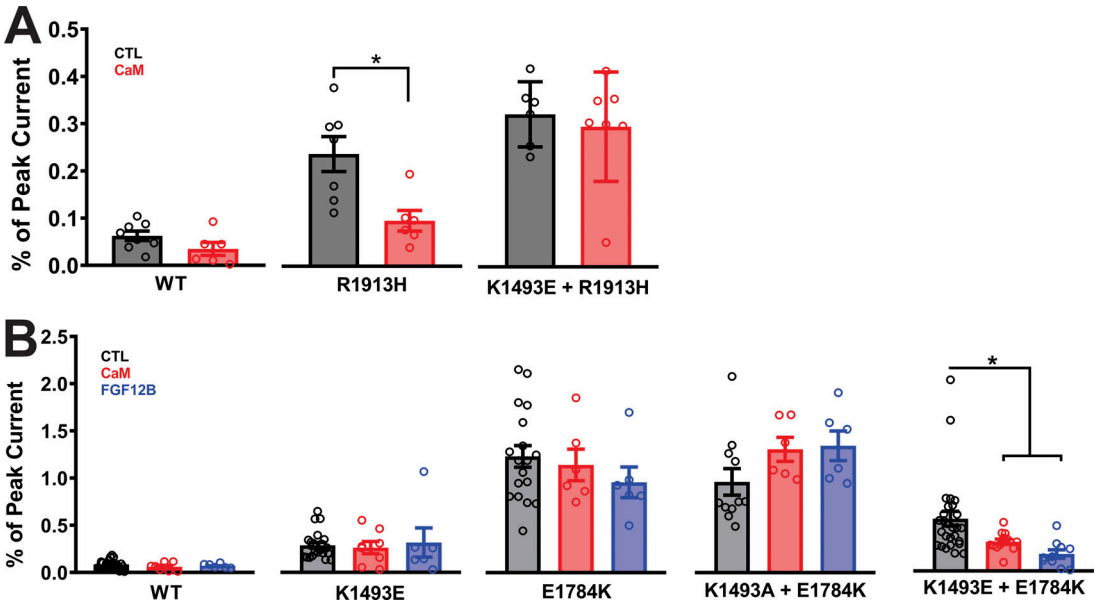

Figure 5. **CaM and FHF modulation of the persistent current is dependent on an intact putative interaction between the III-IV linker and the CTD.** Black represents control, red represents addition of CaM overexpression, and blue represents addition of FGF12B overexpression in A and B). **(A)** Quantified data after overexpression of CaM show failure to rescue persistent currents in R1913H+K1493E. **(B)** CaM and FHF overexpression failed to rescue persistent currents for mutations on either side of the interaction site after overexpression of CaM and FGF12B. Gray columns with black outline in B represent the control data from WT and mutant channels from Fig. 3. *, $P < 0.05$.

(Kapplinger et al., 2015). The E1784K mutant also displayed a large increase in the persistent Na^+ current compared with WT $Na_V1.5$ (Fig. 3, C and D). We then eliminated the positive charge at amino acid 1493 in the context of the E1784K mutation by replacing the endogenous Lys with the Ile found in Na_VPas (K1493I). This second mutation markedly decreased the persistent Na^+ current (Fig. 3, C and D) observed for E1784K alone. Mutating Lys at 1493 to Glu (K1493E), which likewise eliminates the positive charge, also reduced the persistent Na^+ current. Interestingly, mutating K1493 to Ala (K1493A) was ineffective in reducing the persistent current in the context of E1784K, suggesting that packing of the side chains between amino acids 1493 and 1784 is critical for stabilization of the interaction. That single mutations on either side of the interaction site produced an increased persistent Na^+ current, and that certain simultaneous mutations on both sides were effective in reducing the elevated persistent current observed for E1784K alone, supported the hypothesis that an interaction between K1493 and E1784 in $Na_V1.5$ regulates the $Na_V1.5$ persistent sodium current and provides further context for E1784K as the most commonly detected LQT3 mutation. Moreover, these functional readouts of the III-IV linker to CTD interaction are supported by biochemical data from Gardill et al. (2018), who reported that a double mutation K1492E/K1493E abolished binding between a recombinant III-IV linker and CTD. We therefore investigated the individual contribution of K1492, which is in close proximity to the cognate structural interaction observed in NavPas, by replacing K1492 with Glu in the WT and E1784K background. Neither of those mutations showed any significant changes in persistent currents when compared with WT and E1784K, respectively (Fig. S5 A). Thus, we conclude that the functional interactions for K1493 dominate over K1492.

Mutations at the putative III-IV linker to CTD interaction site result in a shift of steady-state inactivation

Perturbation of the III-IV linker function was also shown to alter the steady-state inactivation properties of the VGSC, and the E1784K mutation was reported to induce a hyperpolarized shift in the steady-state inactivation properties (Makita et al., 2008; Peters et al., 2017; Wei et al., 1999). We next sought to determine if the interaction between the III-IV linker and the CTD affects steady-state inactivation. Consistent with the previous reports, E1784K showed a significant hyperpolarized shift in the steady-state inactivation (Fig. 4, A and B). Additionally, K1493E showed a significant hyperpolarized shift in the steady-state inactivation of the channel. However, K1493I and K1493A did not cause a significant shift (Fig. 4, C and D), consistent with the lack of an effect on persistent current (see Fig. 3, A and B). Moreover, all the three mutations on the III-IV linker (K1493I, K1493A, and K1493E) significantly rescued the hyperpolarized shift in the context of E1784K mutations (Fig. 4, C and D; and Table 1). As reported previously, E1784K showed a faster time constant for fast inactivation compared with WT (Peters et al., 2017). In contrast, the time constant for fast inactivation was unaffected for the mutations on the III-IV linker (Fig. S6). These data offer additional support to the hypothesis that the III-IV linker to CTD interaction regulates VGSC inactivation.

Effects of CaM in restoring pathogenic persistent currents depend on an intact interaction between the III-IV linker and the CTD

With this platform, we then investigated whether the interaction between the III-IV linker and the CTD is necessary for CaM and FHF to regulate persistent current. Previous experiments

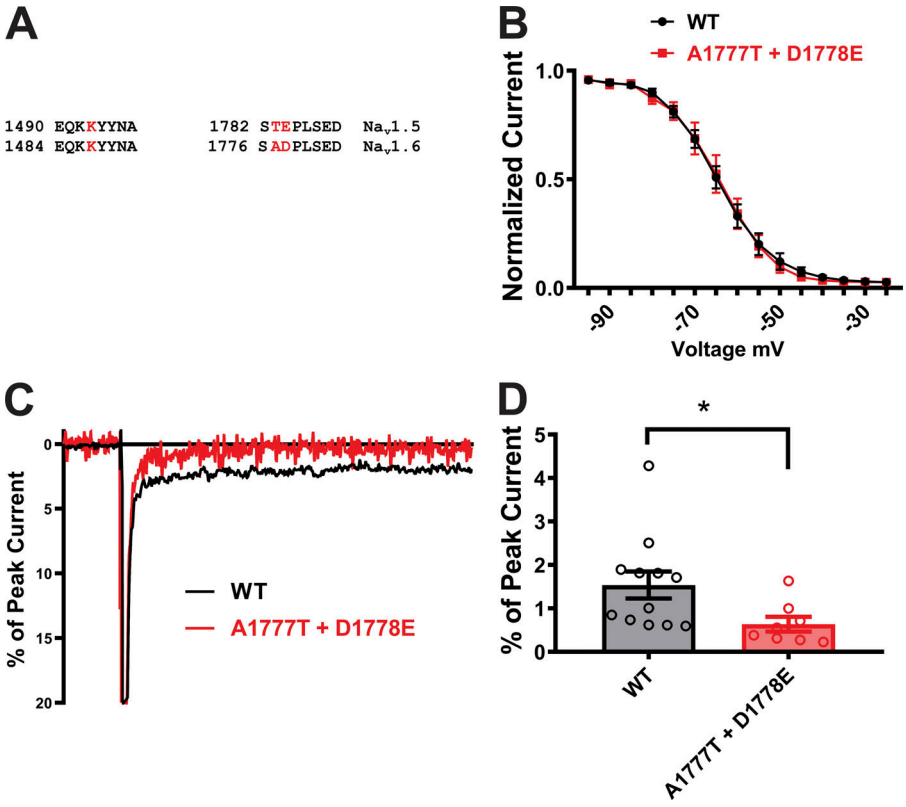

Figure 6. **Mutations at the putative interaction site alter persistent currents in Na$_V$1.6.** **(A)** Sequence homology at the putative interaction sites on the III-IV linker and CTD in Na$_V$1.5 and Na$_V$1.6 channels. **(B)** Exemplar traces displaying the persistent current in WT and mutant channels of Na$_V$1.6. **(C)** Steady-state inactivation curves from WT and mutant channels. **(D)** Quantified data of persistent current in WT and mutant Na$_V$1.6 channels. *, P < 0.05.

demonstrated that CaM overexpression could reduce the persistent current for LQT3 mutations within the CTD, such as R1913H (Yan et al., 2017a). We extended that finding by testing whether the efficacy of CaM on the R1913H mutant Na$_V$1.5 channels depended on the interaction between the III-IV linker and the CTD. As previously observed, overexpression of CaM significantly reduced the persistent current conferred by R1913H (Fig. 5 A). However, when tested in the context of the K1493E mutation that disrupts the interaction between the III-IV linker and the CTD, CaM was no longer effective (Fig. 5 A). Note that CaM was also ineffective at reducing the persistent current for K1493E alone (see Fig. 5 B). Thus, reduction by CaM of persistent current due to CTD mutations appears to require the III-IV linker to CTD interaction. Further supporting evidence was provided by testing the efficacy of CaM on mutations in CTD designed to disrupt interaction with the III-IV linker. For example, we tested whether CaM overexpression could reduce the persistent current observed in E1784K mutant Na$_V$1.5 channels and as shown in Fig. 5 B and found it did not. Thus, for single mutations on either side of the III-IV linker to CTD interaction that conferred increased persistent current, overexpression of CaM was ineffective in reducing the persistent current. We then focused on the set of double mutants previously analyzed. For K1493A+E1784K, which retains a large persistent current and a hypothesized disrupted interaction between the III-IV linker and the CTD, CaM overexpression was likewise ineffective (Fig. 5 B). In contrast, for the double mutant K1493E+E1784K, for which we observed reduced persistent current compared with E1784K alone and which we hypothesize partially restored the interaction between the III-IV linker and CTD, CaM overexpression did reduce the persistent current. FGF12B overexpression produced an identical pattern for the mutants tested, showing efficacy only when the III-IV linker to CTD interaction was intact or restored. Thus, CaM and FGF12B reduced persistent current under conditions in which the interaction between the III-IV linker and the CTD was not completely disrupted. It is possible that there are other interaction sites between the III-IV linker and CTD that are critical for inactivation. One such interaction was suggested by Gardill et al. (2018) between K1504/K1505 on the III-IV linker and Y1795 on the CTD, based on the isothermal titration calorimetry and NMR data. We focused our attention on K1505, a known site for LQT3 mutation (Kapplinger et al., 2015). K1505N channels displayed an increase in the persistent currents that was reduced by overexpression of CaM and FHF. In contrast, although K1505E channels also displayed a higher persistent current, overexpression of CaM or FHF did not rescue the mutant's persistent current (Fig. S5, C and D). The contrasting rescue effects for the milder lysine to asparagine K1505N mutation compared with the charge swap lysine to aspartate K1505E mutation are consistent with biochemical data that showed a marked reduction in the affinity between the III-IV linker and CTD interaction when the III-IV linker contained a K1505E mutation (Gardill et al., 2018). The overexpression of CaM or the addition of FHF is therefore insufficient to overcome that reduced affinity.

A1775T+D1776E mutation in Na$_V$1.6 decreases the persistent currents

To test whether the significance of this III-IV linker to CTD interaction extended beyond Na$_V$1.5, we analyzed the sequence in

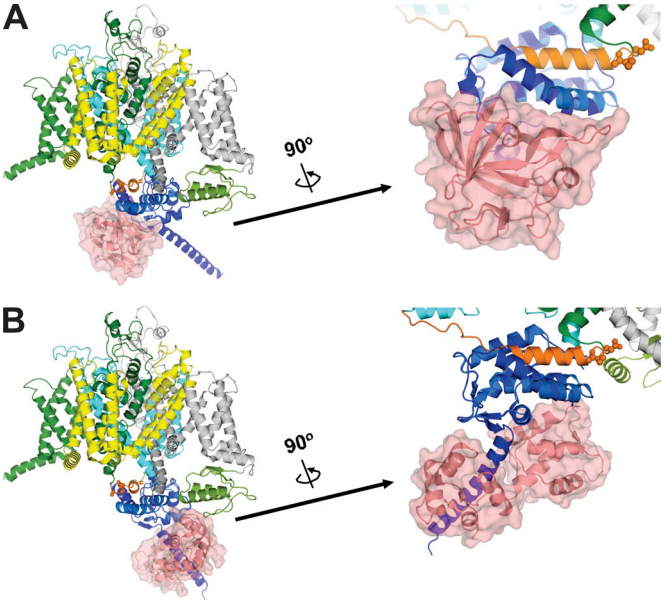

Figure 7. **Models demonstrating a potential mechanism involved in the CaM and FHF modulation of the persistent current mediated through the putative interaction between III-IV linker and CTD.** Structures of the CTD complexes containing FHF/CaM or CaM only overlaid on Na_VPas show FHF (A) and CaM (B) positioned on CTD to stabilize the interaction between III-IV linker and CTD. **(A)** Structure of Na_VPas (PDB accession no. 5X0M) overlaid with the $Na_V1.5$ CTD in complex with FGF13 (PDB accession no. 4DCK). **(B)** Structure of Na_VPas overlaid with the $Na_V1.5$ CTD in complex with CaM (PDB accession no. 4OVN).

other VGSCs. The $Na_V1.6$ VGSC has a large physiological persistent current (Raman and Bean, 1997; Raman et al., 1997), which, like pathological $Na_V1.5$ persistent current, can be reduced by overexpression of CaM (Yan et al., 2017a). As previously hypothesized, one contributor to the increased persistent current seen in $Na_V1.6$ is likely the reduced affinity of CaM for the $Na_V1.6$ CTD compared with the $Na_V1.5$ CTD (Yan et al., 2017a). After investigating the conservation of sequences surrounding the critical E1784 and K1493 equivalents among all human VGSCs, we suspected that destabilization of the III-IV linker to CTD interaction also influenced the physiological increased persistent current in $Na_V1.6$. As shown in Fig. 1 B and Fig. 6 A, K1493 is identical across all human VGSCs. E1784 is also preserved, with the exception of a conservative replacement of the Glu in $Na_V1.5$ by Asp in $Na_V1.6$ (D1778) and in $Na_V1.9$ (D1616). Interestingly, $Na_V1.9$ also displays an unusually large persistent current compared with other VGSCs (Dib-Hajj et al., 2002). Although the change from Glu (at position 1784 in $Na_V1.5$) to Asp (at position 1778 in $Na_V1.6$) is subtle, our data suggested that even slight changes in the interaction between the III-IV linker and the CTD can affect persistent Na^+ current. Thus, we mutated $Na_V1.6$ (D1778E), as well as the adjacent A1777T, to the cognate amino acids found in $Na_V1.5$ and tested the consequence on persistent current. The $Na_V1.6$ double mutant (A1777T+D1778E) displayed significantly lower persistent currents compared with the WT $Na_V1.6$ channel, emphasizing the influence of III-IV linker to CTD interaction across subtypes of VGSCs (Fig. 6, B–D). These subtle mutations in $Na_V1.6$ did not influence the $V_{1/2}$ of inactivation, however, suggesting a specific role in persistent current (Fig. 6 C).

Discussion

Persistent sodium current may result from failure of the VGSC to inactivate, reentry of the channel into the open state after inactivation, or destabilization of the closed state. Although the III-IV linker is identified as the principal inactivation gate responsible for fast inactivation in VGSCs, a role for CTD-interacting channel auxiliary subunits, such as CaM and FHFs, in regulating inactivation properties is indicated by mutations that reduce the binding affinity of CaM or FHFs to the CTD and lead to increased persistent Na^+ channel currents (Musa et al., 2015; Yan et al., 2017a). The increased persistent current associated with these mutations can be rescued by overcoming the reduced binding through overexpression of CaM or FHF (Musa et al., 2015; Yan et al., 2017a). Deletion of the isoleucine glutamine (IQ) motif in the CTD (thereby eliminating the apoCaM binding site) or mutating the FHF to prevent CTD interaction abolished the effects of overexpression of CaM or an FHF (Fig. 2), emphasizing that these auxiliary subunits exert their influence on persistent current through interaction with the CTD. Here, building on recent structural information, we propose that these auxiliary subunits act on the CTD, as observed in the Na_VPas structure, and stabilizing the CTD's interaction with the III-IV linker.

We examined this in Fig. 7, A and B, by overlaying structures of the $Na_V1.5$ CTD on the Na_VPas structure. As previously noted, the portion of the CTD visualized in Na_VPas cryo-EM structure (proximal to the predicted IQ motif helix) was modeled after the analogous region in the $Na_V1.5$ CTD from the crystal structure of a ternary complex (4DCK) obtained in the absence of Ca^{2+} and containing the $Na_V1.5$ CTD, CaM, and FGF13 (Shen et al., 2017; Wang et al., 2012). Overlaying that ternary complex on Na_VPas places FGF13 below the CTD (Fig. 7 A), thus cradling the III-IV linker "hot dog" in the CTD "bun" (see also Fig. 1). Thus, we hypothesize that the presence of the FHF promotes and stabilizes the III-IV linker to CTD interaction seen in the closed state. In our experiments focusing on the role of CaM (e.g., Fig. 5), we did not express an FHF, and there is no endogenous FHF expressed in HEK293 cells. Because the absence of an FHF induces a 90° twist between the proximal $Na_V1.5$ CTD and the CaM binding IQ motif, and alters the CaM interaction with the $Na_V1.5$ CTD (Gabelli et al., 2014; Pitt and Lee, 2016), we modeled the effects of CaM by instead overlaying a crystal structure of a $Na_V1.5$ CTD in complex with apoCaM (PDB accession no. 4OVN; Gabelli et al., 2014) on Na_VPas (Fig. 7 B). This places the apoCaM N-lobe adjacent to the CTD and, analogous to the model for FGF13, appears to stabilize the CTD to III-IV linker interaction in the closed state.

The interaction between the III-IV linker and the CTD is dynamic, as demonstrated by the marked shift in position of the III-IV linker observed in the inactivated state (Pan et al., 2018). Building on this and structures of chimeric channels generated by inserting the $Na_V1.7$ domain IV voltage sensor into NavPas with and without the addition of α-scorpion toxin that allow

comparison of a presumed transitional closed state and a deactivated state, Clairfeuille et al. (2019) propose the III-IV linker remains restrained by the CTD by two "switch" domains. The E1784 residue studied here is a component of "switch 2." Upon domain IV voltage sensor activation, the switch domains sequentially unfetter the III-IV linker, allowing it to begin its transformation to its inactivated state position. As noted by those authors, mutations in the switches across several Na_V isoforms lead to an increase in persistent Na^+ current. We hypothesize that CaM and FHFs associated with the CTD participate in restraining the III-IV linker through sites like switch 2, thus rationalizing why mutations that affect CaM or FHF interaction with the CTD likewise lead to increased persistent Na^+ current. In the absence of structures caught in other transition states and the absence of relevant structures that contain a more complete CTD with CaM and FHF bound, we hypothesize that perturbation of CaM or FHF interaction with the CTD affects the III-IV linker to decrease the probability that it will efficiently transition to its inactivated position.

Our functional data using the modified $Na_V1.6$ channel and its consequent effects on Na^+ persistent current further support the conservation of the III-IV linker to CTD interaction among various VGSC isoforms. Moreover, our data provide a basis for understanding how subtle differences even among the highly conserved sequences across the VGSCs subtypes correlate with marked differences in physiological higher persistent current, such as seen in $Na_V1.6$ and $Na_V1.9$. The mutations within switch 2 significantly decreased the persistent currents in the $Na_V1.6$ that we modified toward a $Na_V1.5$-like switch 2, likely underling the importance of switch 1 and other factors, such as the lower CaM-binding affinity to the $Na_V1.6$ CTD compared with $Na_V1.5$.

In addition to effects on persistent current, the cryo-EM Na_VPas and Na_VPas chimera structures provide insight into the mechanisms underlying the hyperpolarized shift in steady-state inactivation. Mutations in switch 1 or switch 2, similar to those we generated in this study, led to a hyperpolarized shift in the steady-state inactivation (Clairfeuille et al., 2019). This is also consistent with a model in which the mutations destabilize the III-IV linker to CTD interaction, leading to premature release of the III-IV linker and entry of the channels into closed-state inactivation, reflected as a hyperpolarized shift in steady-state inactivation (Chanda and Bezanilla, 2002; Capes et al., 2013). We hypothesize that its interaction with CTD provides a barrier for the III-IV linker, preventing premature inactivation. However, unlike for persistent currents, these effects are not mediated through CaM interaction at CTD as overexpression of CaM did not alter the steady-state inactivation of any of the mutant tested (Table 1).

In summary, our data reveal a structure-guided identification of a putative functional interaction site between CTD and III-IV linker. Alteration of this interaction site leads to perturbed Na^+ channel inactivation properties. Moreover, we predict that this interaction between the CTD and the III-IV linker provides an explanation for how mutations in the CTD confer pathogenic increased persistent current, and how auxiliary subunits associated with the CTD, apoCaM and FHFs, contribute to the regulation of inactivation. Finally, our data also shed new light on the underlying mechanism for E1784K, the most commonly reported LQT3 mutation.

Acknowledgments

Richard W. Aldrich served as editor.

Supported by National Institutes of Health grant R01 HL71165 (G.S. Pitt) and National Institutes of Health grant R01 HL122967 (G.S. Pitt and S.O. Marx).

The authors declare no competing financial interests.

Author contributions: A.R. Gade, S.O. Marx, and G.S. Pitt designed experiments. A.R. Gade performed experiments. A.R. Gade and G.S. Pitt analyzed data. A.R. Gade, S.O. Marx, and G.S. Pitt wrote the manuscript.

Submitted: 1 July 2019
Accepted: 25 November 2019

References

Bennett, P.B., K. Yazawa, N. Makita, and A.L. George Jr. 1995. Molecular mechanism for an inherited cardiac arrhythmia. *Nature.* 376:683–685. https://doi.org/10.1038/376683a0

Biswas, S., D. DiSilvestre, Y. Tian, V.L. Halperin, and G.F. Tomaselli. 2009. Calcium-mediated dual-mode regulation of cardiac sodium channel gating. *Circ. Res.* 104:870–878. https://doi.org/10.1161/CIRCRESAHA.108.193565

Capes, D.L., M.P. Goldschen-Ohm, M. Arcisio-Miranda, F. Bezanilla, and B. Chanda. 2013. Domain IV voltage-sensor movement is both sufficient and rate limiting for fast inactivation in sodium channels. *J. Gen. Physiol.* 142:101–112. https://doi.org/10.1085/jgp.201310998

Catterall, W.A. 2000. From ionic currents to molecular mechanisms: the structure and function of voltage-gated sodium channels. *Neuron.* 26:13–25. https://doi.org/10.1016/S0896-6273(00)81133-2

Catterall, W.A., A.L. Goldin, and S.G. Waxman. 2005. International Union of Pharmacology. XLVII. Nomenclature and structure-function relationships of voltage-gated sodium channels. *Pharmacol. Rev.* 57:397–409. https://doi.org/10.1124/pr.57.4.4

Chanda, B., and F. Bezanilla. 2002. Tracking voltage-dependent conformational changes in skeletal muscle sodium channel during activation. *J. Gen. Physiol.* 120:629–645. https://doi.org/10.1085/jgp.20028679

Choi, J.I., C. Wang, M.J. Thomas, and G.S. Pitt. 2016. α1-Syntrophin Variant Identified in Drug-Induced Long QT Syndrome Increases Late Sodium Current. *PLoS One.* 11:e0152355. https://doi.org/10.1371/journal.pone.0152355

Clairfeuille, T., A. Cloake, D.T. Infield, J.P. Llongueras, C.P. Arthur, Z.R. Li, Y. Jian, M.F. Martin-Eauclaire, P.E. Bougis, C. Ciferri, et al. 2019. Structural basis of alpha-scorpion toxin action on Nav channels. *Science.* 363:eaav8573.

Cormier, J.W., I. Rivolta, M. Tateyama, A.S. Yang, and R.S. Kass. 2002. Secondary structure of the human cardiac Na+ channel C terminus: evidence for a role of helical structures in modulation of channel inactivation. *J. Biol. Chem.* 277:9233–9241. https://doi.org/10.1074/jbc.M110204200

Dib-Hajj, S., J.A. Black, T.R. Cummins, and S.G. Waxman. 2002. NaN/Nav1.9: a sodium channel with unique properties. *Trends Neurosci.* 25:253–259. https://doi.org/10.1016/S0166-2236(02)02150-1

Gabelli, S.B., A. Boto, V.H. Kuhns, M.A. Bianchet, F. Farinelli, S. Aripirala, J. Yoder, J. Jakoncic, G.F. Tomaselli, and L.M. Amzel. 2014. Regulation of the NaV1.5 cytoplasmic domain by calmodulin. *Nat. Commun.* 5:5126. https://doi.org/10.1038/ncomms6126

Gardill, B.R., R.E. Rivera-Acevedo, C.C. Tung, M. Okon, L.P. McIntosh, and F. Van Petegem. 2018. The voltage-gated sodium channel EF-hands form an interaction with the III-IV linker that is disturbed by disease-causing mutations. *Sci. Rep.* 8:4483. https://doi.org/10.1038/s41598-018-22713-y

Gellens, M.E., A.L. George Jr., L.Q. Chen, M. Chahine, R. Horn, R.L. Barchi, and R.G. Kallen. 1992. Primary structure and functional expression of the human cardiac tetrodotoxin-insensitive voltage-dependent sodium

channel. *Proc. Natl. Acad. Sci. USA.* 89:554–558. https://doi.org/10.1073/pnas.89.2.554

Johnson, C.N., F. Potet, M.K. Thompson, B.M. Kroncke, A.M. Glazer, M.W. Voehler, B.C. Knollmann, A.L. George, Jr., and W.J. Chazin. 2018. A Mechanism of Calmodulin Modulation of the Human Cardiac Sodium Channel. *Structure.* 26:683–694.e3.

Kapplinger, J.D., J.R. Giudicessi, D. Ye, D.J. Tester, T.E. Callis, C.R. Valdivia, J.C. Makielski, A.A. Wilde, and M.J. Ackerman. 2015. Enhanced Classification of Brugada Syndrome-Associated and Long-QT Syndrome-Associated Genetic Variants in the SCN5A-Encoded Na(v)1.5 Cardiac Sodium Channel. *Circ Cardiovasc Genet.* 8:582–595. https://doi.org/10.1161/CIRCGENETICS.114.000831

Makita, N., E. Behr, W. Shimizu, M. Horie, A. Sunami, L. Crotti, E. Schulze-Bahr, S. Fukuhara, N. Mochizuki, T. Makiyama, et al. 2008. The E1784K mutation in SCN5A is associated with mixed clinical phenotype of type 3 long QT syndrome. *J. Clin. Invest.* 118:2219–2229.

Meisler, M.H., and J.A. Kearney. 2005. Sodium channel mutations in epilepsy and other neurological disorders. *J. Clin. Invest.* 115:2010–2017. https://doi.org/10.1172/JCI25466

Motoike, H.K., H. Liu, I.W. Glaaser, A.S. Yang, M. Tateyama, and R.S. Kass. 2004. The Na+ channel inactivation gate is a molecular complex: a novel role of the COOH-terminal domain. *J. Gen. Physiol.* 123:155–165. https://doi.org/10.1085/jgp.200308929

Musa, H., C.F. Kline, A.C. Sturm, N. Murphy, S. Adelman, C. Wang, H. Yan, B.L. Johnson, T.A. Csepe, A. Kilic, et al. 2015. SCN5A variant that blocks fibroblast growth factor homologous factor regulation causes human arrhythmia. *Proc. Natl. Acad. Sci. USA.* 112:12528–12533. https://doi.org/10.1073/pnas.1516430112

Nof, E., L. Vysochek, E. Meisel, E. Burashnikov, C. Antzelevitch, J. Clatot, R. Beinart, D. Luria, M. Glikson, and S. Oz. 2019. Mutations in $Na_V1.5$ Reveal Calcium-Calmodulin Regulation of Sodium Channel. *Front. Physiol.* 10:700. https://doi.org/10.3389/fphys.2019.00700

Pablo, J.L., C. Wang, M.M. Presby, and G.S. Pitt. 2016. Polarized localization of voltage-gated Na+ channels is regulated by concerted FGF13 and FGF14 action. *Proc. Natl. Acad. Sci. USA.* 113:E2665–E2674. https://doi.org/10.1073/pnas.1521194113

Pan, X., Z. Li, Q. Zhou, H. Shen, K. Wu, X. Huang, J. Chen, J. Zhang, X. Zhu, J. Lei, et al. 2018. Structure of the human voltage-gated sodium channel $Na_v1.4$ in complex with β1. *Science.* 362:eaau2486. https://doi.org/10.1126/science.aau2486

Pan, X., Z. Li, X. Huang, G. Huang, S. Gao, H. Shen, L. Liu, J. Lei, and N. Yan. 2019. Molecular basis for pore blockade of human Na^+ channel $Na_v1.2$ by the μ-conotoxin KIIIA. *Science.* 363:1309–1313. https://doi.org/10.1126/science.aaw2999

Patton, D.E., J.W. West, W.A. Catterall, and A.L. Goldin. 1992. Amino acid residues required for fast Na(+)-channel inactivation: charge neutralizations and deletions in the III-IV linker. *Proc. Natl. Acad. Sci. USA.* 89:10905–10909. https://doi.org/10.1073/pnas.89.22.10905

Peters, C.H., A. Yu, W. Zhu, J.R. Silva, and P.C. Ruben. 2017. Depolarization of the conductance-voltage relationship in the NaV1.5 mutant, E1784K, is due to altered fast inactivation. *PLoS One.* 12:e0184605. https://doi.org/10.1371/journal.pone.0184605

Pitt, G.S., and S.Y. Lee. 2016. Current view on regulation of voltage-gated sodium channels by calcium and auxiliary proteins. *Protein Sci.* 25:1573–1584. https://doi.org/10.1002/pro.2960

Raman, I.M., and B.P. Bean. 1997. Resurgent sodium current and action potential formation in dissociated cerebellar Purkinje neurons. *J. Neurosci.* 17:4517–4526. https://doi.org/10.1523/JNEUROSCI.17-12-04517.1997

Raman, I.M., L.K. Sprunger, M.H. Meisler, and B.P. Bean. 1997. Altered subthreshold sodium currents and disrupted firing patterns in Purkinje neurons of Scn8a mutant mice. *Neuron.* 19:881–891. https://doi.org/10.1016/S0896-6273(00)80969-1

Sarhan, M.F., C.C. Tung, F. Van Petegem, and C.A. Ahern. 2012. Crystallographic basis for calcium regulation of sodium channels. *Proc. Natl. Acad. Sci. USA.* 109:3558–3563. https://doi.org/10.1073/pnas.1114748109

Shen, H., Q. Zhou, X. Pan, Z. Li, J. Wu, and N. Yan. 2017. Structure of a eukaryotic voltage-gated sodium channel at near-atomic resolution. *Science.* 355:eaal4326. https://doi.org/10.1126/science.aal4326

Shen, H., Z. Li, Y. Jiang, X. Pan, J. Wu, B. Cristofori-Armstrong, J.J. Smith, Y.K.Y. Chin, J. Lei, Q. Zhou, et al. 2018. Structural basis for the modulation of voltage-gated sodium channels by animal toxins. *Science.* 362:eaau2596. https://doi.org/10.1126/science.aau2596

Shen, H., D. Liu, K. Wu, J. Lei, and N. Yan. 2019. Structures of human $Na_v1.7$ channel in complex with auxiliary subunits and animal toxins. *Science.* 363:1303–1308. https://doi.org/10.1126/science.aaw2493

Wang, Q., J. Shen, I. Splawski, D. Atkinson, Z. Li, J.L. Robinson, A.J. Moss, J.A. Towbin, and M.T. Keating. 1995. SCN5A mutations associated with an inherited cardiac arrhythmia, long QT syndrome. *Cell.* 80:805–811. https://doi.org/10.1016/0092-8674(95)90359-3

Wang, C., C. Wang, E.G. Hoch, and G.S. Pitt. 2011. Identification of novel interaction sites that determine specificity between fibroblast growth factor homologous factors and voltage-gated sodium channels. *J. Biol. Chem.* 286:24253–24263. https://doi.org/10.1074/jbc.M111.245803

Wang, C., B.C. Chung, H. Yan, S.Y. Lee, and G.S. Pitt. 2012. Crystal structure of the ternary complex of a NaV C-terminal domain, a fibroblast growth factor homologous factor, and calmodulin. *Structure.* 20:1167–1176. https://doi.org/10.1016/j.str.2012.05.001

Wang, C., B.C. Chung, H. Yan, H.G. Wang, S.Y. Lee, and G.S. Pitt. 2014. Structural analyses of Ca^{2+}/CaM interaction with NaV channel C-termini reveal mechanisms of calcium-dependent regulation. *Nat. Commun.* 5:4896. https://doi.org/10.1038/ncomms5896

Wei, J., D.W. Wang, M. Alings, F. Fish, M. Wathen, D.M. Roden, and A.L. George Jr. 1999. Congenital long-QT syndrome caused by a novel mutation in a conserved acidic domain of the cardiac Na+ channel. *Circulation.* 99:3165–3171. https://doi.org/10.1161/01.CIR.99.24.3165

West, J.W., D.E. Patton, T. Scheuer, Y. Wang, A.L. Goldin, and W.A. Catterall. 1992. A cluster of hydrophobic amino acid residues required for fast Na(+)-channel inactivation. *Proc. Natl. Acad. Sci. USA.* 89:10910–10914. https://doi.org/10.1073/pnas.89.22.10910

Wu, L., J. Ma, H. Li, C. Wang, E. Grandi, P. Zhang, A. Luo, D.M. Bers, J.C. Shryock, and L. Belardinelli. 2011. Late sodium current contributes to the reverse rate-dependent effect of IKr inhibition on ventricular repolarization. *Circulation.* 123:1713–1720. https://doi.org/10.1161/CIRCULATIONAHA.110.000661

Yan, H., C. Wang, S.O. Marx, and G.S. Pitt. 2017a. Calmodulin limits pathogenic Na+ channel persistent current. *J. Gen. Physiol.* 149:277–293. https://doi.org/10.1085/jgp.201611721

Yan, Z., Q. Zhou, L. Wang, J. Wu, Y. Zhao, G. Huang, W. Peng, H. Shen, J. Lei, and N. Yan. 2017b. Structure of the Nav1.4-beta1 Complex from Electric Eel. *Cell.* 170:470–482.e11.

Zumhagen, S., M.W. Veldkamp, B. Stallmeyer, A. Baartscheer, L. Eckardt, M. Paul, C.A. Remme, Z.A. Bhuiyan, C.R. Bezzina, and E. Schulze-Bahr. 2013. A heterozygous deletion mutation in the cardiac sodium channel gene SCN5A with loss- and gain-of-function characteristics manifests as isolated conduction disease, without signs of Brugada or long QT syndrome. *PLoS One.* 8:e67963. https://doi.org/10.1371/journal.pone.0067963